Global Wind-Induced Change of Deep-Sea Sediment Budgets, New Ocean Production and CO$_2$ Reservoirs ca. 3.3-2.35 Ma BP

M. Sarnthein and J. Fenner

Email alerting service	Receive free email alerts when new articles cite this article - sign up in the box at the top right-hand corner of the article or click **here**

To subscribe to *Phil. Trans. R. Soc. Lond. B* go to: **http://rstb.royalsocietypublishing.org/subscriptions**

Global wind-induced change of deep-sea sediment budgets, new ocean production and CO_2 reservoirs *ca.* 3.3–2.35 Ma BP

By M. Sarnthein and J. Fenner

Geologisch-Palaeontologisches Institut, Universität Kiel, Olshausenstrasse 40,
*D-*2300 *Kiel, F.R.G.*

The late Pliocene phase of large-scale climatic deterioration about 3.2–2.4 Ma BP is well documented in a number of (benthic) $\delta^{18}O$ records. To test the global implications of this event, we have mapped the distribution patterns of various sediment variables in the Pacific and Atlantic Oceans during two time slices, 3.4–3.18 and 2.43–2.33 Ma BP. The changes of bulk sedimentation and bulk sediment accumulation rates are largely explained by the variations of $CaCO_3$-accumulation rates (and the accumulation rates of the complementary siliciclastic sediment fraction near continents in higher latitudes).

During the late Pliocene, the $CaCO_3$-accumulation rate increased along the equatorial Pacific and Atlantic and in the northeastern Atlantic, but decreased elsewhere. The accumulation rate of organic carbon (C_{org}) and net palaeoproductivity also increased below the high-productivity belts along the equator and the eastern continental margins. From these patterns we may conclude that (trade-) wind-induced upwelling zones and upwelling productivity were much enhanced during that time. This change led to an increased transfer of CO_2 from the surface ocean to the ocean deep water and to a reduction of evaporation, which resulted in an aridification of the Saharan desert belt as depicted in the dust sediments off north-west Africa.

Introduction

Various lines of recently compiled evidence from sediments of the North Atlantic suggest that the Quaternary régime of pronounced climatic fluctuations and glaciations started at about 2.5 Ma BP, after a fairly short phase of massive climatic deterioration during the Late Pliocene, i.e. a major 'event' perhaps comparable with that of the Middle Miocene and that near the Eocene–Oligocene boundary.

The first and major evidence for this was based on the few detailed benthic $\delta^{18}O$ curves available from the depth range of North Atlantic Deep Water (NADW) between about 2800 and 4100 m (figure 1). These records of the Deep Sea Drilling Project (DSDP) Sites (141), 366, 397 and 552 reveal a Late Tertiary 'golden age' of stable climate, which was almost free of cold fluctuations and lasted until about 3.2 Ma BP. Subsequently, the fluctuations increased rapidly and had reached a first fully developed glacial amplitude by 2.43–2.33 Ma BP, with a magnitude comparable to those of the Early Quaternary before *ca.* 1 Ma BP.

Further evidence for major environmental changes during that time was obtained from site 397 (Stein 1984, 1985) offshore from the northwestern Saharan coast (27° N). At this site, the sediment composition after 3.0 Ma BP, and especially after 2.43 Ma BP, records a significant increase in the concentration of biogenic opal and in the accumulation rate of organic carbon, which both form reliable records of enhanced ocean carbon productivity (figure 2). The lower part of the section with enhanced palaeoproductivity was also marked by a substantial supply
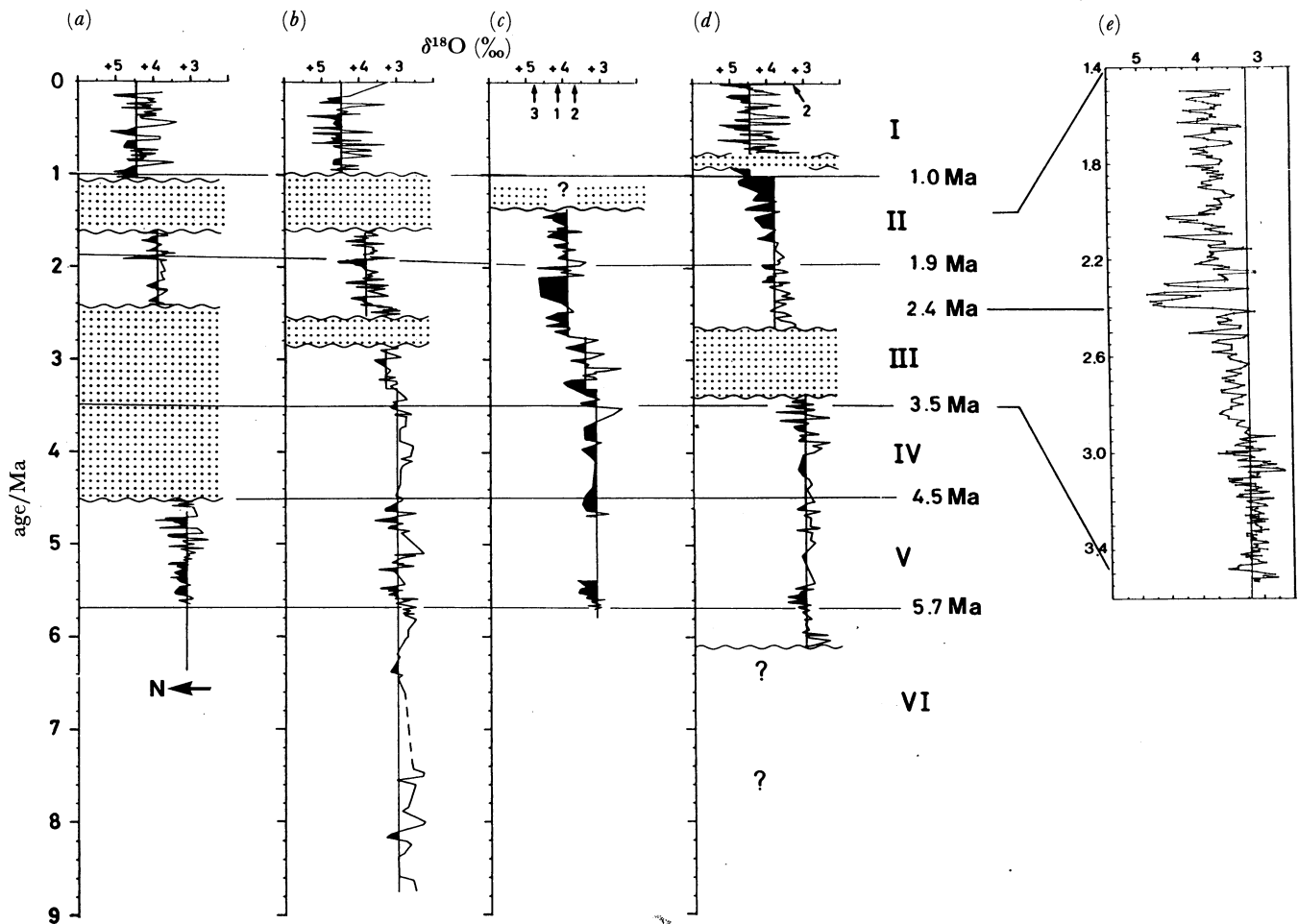
[77]

FIGURE 1. Benthos $\delta^{18}O$ records from DSDP sites 544B (a), 141 (c) and 366 (Stein 1984) (d), 397 (Shackleton & Cita 1979; supplemented by Stein 1984) (b) and 552 (Shackleton & Hall 1985) (e).

of fluvial mud. It was replaced by aeolian dust only after 2.38 Ma BP. This has two implications. One is the onset of strong aridity in the north Sahara during that time; the other is an ambiguity in interpreting the early phase of enhanced near-shore productivity. It may either be controlled by more intensive coastal upwelling or by stronger fertilization owing to fluvial discharge, as would happen, for example, if the sea level were lowered. Recent results (Ruddiman *et al.* 1987) from Ocean Drilling Project (ODP) site 658 off Cap Blanc (22° N) suggest a decrease in the fluvial sediment supply as early as *ca.* 3.0 Ma BP, i.e. they imply that upwelling is the main factor influencing primary productivity in that region.

A third, independent line of evidence for major changes in the ocean palaeoenvironment

FIGURE 2. Late Pliocene climatic deterioration as depicted by benthos $\delta^{18}O$ (a) and the variations of the sedimentary régime off northwest Africa (27° N) (data from DSDP site 397; modified and supplemented from Stein (1984, 1985)): concentrations (as percentage of carbonate-free sediment fraction over 6 μm) of biogenic opal (b); accumulation rates of organic carbon (c); accumulation rates of siliciclastic sediment fraction (grain size over 6 μm) (d); and palaeowind speeds (e) as deduced from aeolian dust-grain diameters via the term l/uz, where l is trajectory length, u is wind speed and z is the diameters thickness of the air mass. Arrows show samples with riverborne terrigenous sediment fraction.
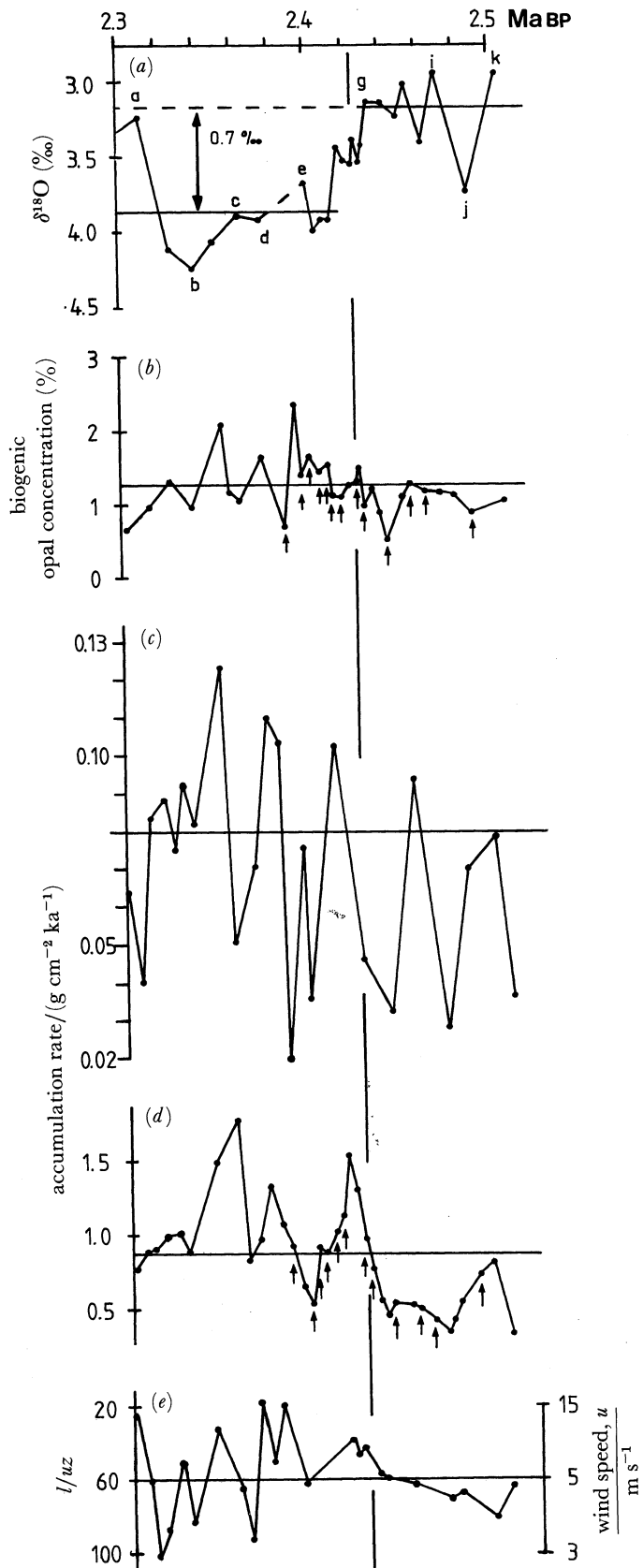
FIGURE 2. For description see opposite.

[79]

about 2.5 Ma BP is obtained from the few benthic $\delta^{13}C$ records of ΣCO_2 in the North Atlantic Deep Water (figure 3), although their dating requires further improvement. For example, $\delta^{13}C$ values decrease at site 366 (mainly from *C. wuellerstorfi*) by approximately 0.2‰ from *ca.* 2.25 to 2.0 Ma BP. At site 397 they decrease by about 0.25‰ (mixed *Uvigerina* and *C. wuellerstorfi* values) after *ca.* 2.5 Ma BP (Stein 1984), and at site 552 by about 0.5‰ from 2.4 to 2.05 Ma BP and also at 3.27–3.08 Ma BP (Shackleton & Hall 1985). Because the latter record is almost
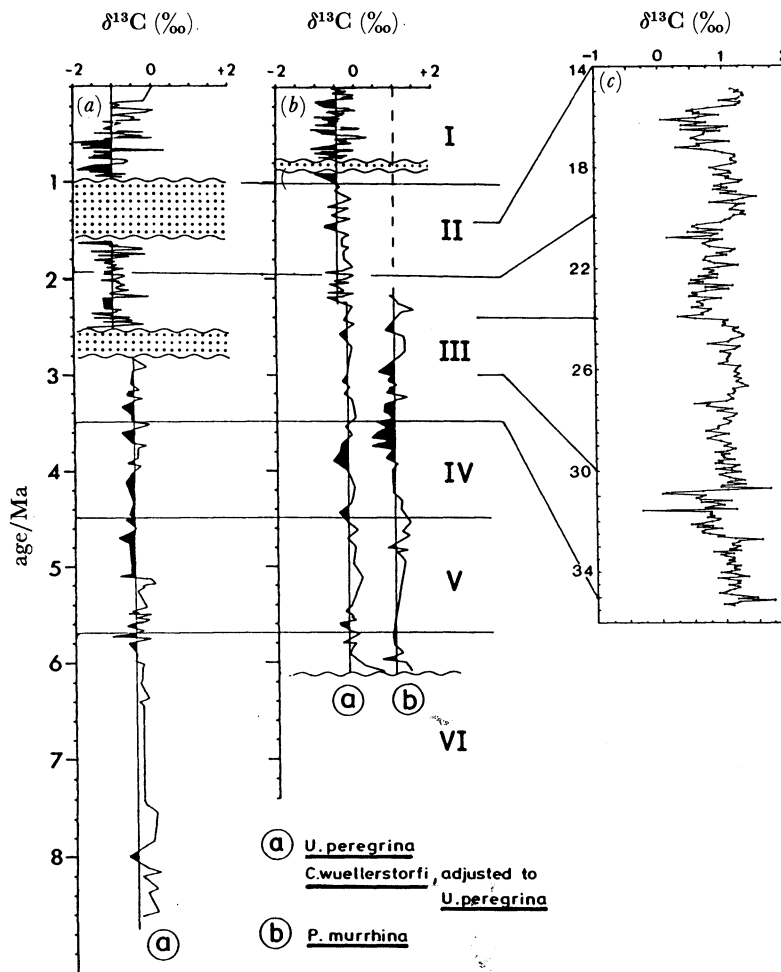

FIGURE 3. Benthos $\delta^{13}C$ records from DSDP sites 366 (Stein 1984) (*b*), 397 (Shackleton & Cita 1979; supplemented by Stein 1984) (*a*) and 552 (Shackleton & Hall 1985) (*c*).

exclusively based on data from *Uvigerina* sp., the more conservative estimate of the difference of about 0.2–0.25‰ $\delta^{13}C$ may be more realistic (Zahn *et al.* 1986). Also this estimate already records an extraction of almost 300 Gt C (calculated after Duplessy (1982) from the surface ocean, atmosphere, and terrestrial biosphere to the deep ocean; this value is almost one half of a modern atmospheric carbon unit (about 650 Gt C). We may assume that the transfer was possibly controlled by an increase in the steady-state flux of particulate organic matter.

To test this model and to contribute generally to a better understanding of the gradually emerging late Pliocene climate 'event', we compare, in this paper, global distribution maps of sediment fluxes and ocean palaeoproductivity from two time intervals, at 3.4–3.18 and

FIGURE 4. Locations of DSDP sites and coring stations used for reconstruction of time intervals described in this paper.

TABLE 1. LOCATION OF SITES

site	locality	geographic latitude	location longitude	water depth m
ATLANTIC				
DSDP 552A	Rockall Plateau	56° 02.56′ N	23° 13.88′ W	2301
610A	Rockall Plateau, Feni Drift	53° 13.30′ N	18° 53.21′ W	2417
611D	Gadar Drift	52° 50.47′ N	30° 18.58′ W	3203
609B	Mid-Atlantic Ridge	49° 52.67′ N	24° 14.29′ W	3884
548	Goban Spur	48° 54.95′ N	12° 09.84′ W	1256
400A	Bay of Biscay	47° 22.90′ N	09° 11.90′ W	4399
608	Kings Trough	42° 50.21′ N	23° 05.25′ W	3526
607	Mid-Atlantic Ridge	41° 00.07′ N	32° 57.44′ W	3427
606	Mid-Atlantic Ridge	37° 20.29′ N	35° 30.01′ W	3007
397	cont. slope off Cape Bojador	26° 50.70′ N	15° 10.80′ W	2900
141	north of Cape Verde Islands	19° 25.16′ N	23° 59.91′ W	4148
541	cont. foot of Barbados Ridge	15° 31.20′ N	58° 43.70′ W	4940
366A	Sierra Leone Rise	05° 40.70′ N	19° 51.10′ W	2853
521	Mid-Atlantic Ridge	26° 04.43′ S	10° 15.87′ W	4125
522	Mid-Atlantic Ridge	26° 06.84′ S	05° 07.78′ W	4441
519	Mid-Atlantic Ridge	26° 08.20′ S	11° 39.97′ W	3769
515A	Brazil Basin	26° 14.31′ S	36° 30.17′ W	4252
523	Angola Basin	28° 33.13′ S	02° 15.08′ W	4562
518	Brazil Basin	29° 58.42′ S	38° 08.12′ W	3944
516A	Rio Grande Rise	30° 16.59′ S	35° 17.10′ W	1313
517	west flank, Rio Grande Rise	30° 56.81′ S	38° 02.47′ W	2963
514	Mid-Atlantic Ridge	46° 02.77′ S	26° 51.30′ W	4318
CARIBBEAN				
DSDP 502C	Columbia Basin	11° 29.48′ N	79° 22.70′ W	3051
PACIFIC OCEAN				
V21-173	NE Pacific	44° 22.00′ N	163° 33.00′ W	5493
RC12-413	NW Pacific	43° 17.00′ N	166° 54.00′ E	5015
V21-148	NW Pacific, abyssal plain	42° 05.00′ N	160° 36.00′ E	5477
RC10-203	central N Pacific	41° 42.00′ N	171° 57.00′ W	5883
DSDP580	NW Pacific, abyssal plain	41° 37.47′ N	153° 58.58′ E	5375
RC12-415	NW Pacific	41° 17.00′ N	164° 09.00′ E	4872
V20-88	central N Pacific	40° 11.00′ N	151° 39.00′ W	—
DSDP440B	Japan Trench, slope terrace	39° 44.13′ N	143° 55.74′ E	4509
DSDP579A	NW Pacific, abyssal plain	38° 37.68′ N	153° 50.17′ E	5737
V20-89	central N Pacific	38° 12.00′ N	153° 35.00′ W	—
DSDP310	Hess Rise	36° 52.11′ N	176° 54.09′ E	3516
V32-127	central N Pacific	35° 28.00′ N	177° 34.00′ E	3927
DSDP578	NW Pacific, abyssal plain	33° 55.56′ N	151° 37.74′ E	6010
DSDP577A	Shatsky Rise	32° 26.53′ N	157° 34.39′ E	2678
DSDP576	NW Pacific, abyssal plain	32° 21.36′ N	164° 16.54′ E	6217
RC12-63	central Pacific	05° 58.00′ N	142° 39.00′ W	4949
DSDP575	eastern equatorial Pacific	05° 51.00′ N	135° 02.16′ W	4536
V28-179	central Pacific	04° 37.00′ N	139° 36.00′ W	4509
DSDP574	eastern equatorial Pacific	04° 12.52′ N	133° 19.81′ W	4561
DSDP503B	eastern equatorial Pacific	04° 03.02′ N	95° 38.32′ W	3672
V24-62	central Pacific	03° 04.00′ N	153° 35.00′ W	4834
V24-60	central Pacific	02° 48.00′ N	149° 00.00′ W	4859
RC12-66	central pacific	02° 36.60′ N	148° 12.80′ W	4755
V24-59	central Pacific	02° 34.00′ N	145° 32.00′ W	4662
KH68-4-18	central Pacific	01° 59.00′ N	170° 01.00′ W	5390
DSDP504	S flank, Costa Rica Rift	01° 13.58′ N	83° 43.93′ W	3460
DSDP573	eastern equatorial Pacific	00° 29.91′ N	133° 18.57′ W	4301
DSDP586B	western equatorial Pacific	00° 29.84′ S	158° 29.89′ E	2208
DSDP157	Carnegie Ridge	01° 45.70′ S	85° 54.17′ W	1591
M70-39	central Pacific	02° 27.00′ S	173° 20.00′ W	5412

TABLE 1. (cont.)

| site	locality	geographic latitude	location longitude	water depth m
KH68-4-20	central Pacific	02° 28.00′ S	170° 00.00′ W	5535
M70-16	central Pacific	03° 13.00′ S	160° 15.00′ W	5543
DSDP587	Landsdowne Bank	21° 11.09′ S	161° 19.99′ E	1101
DSDP588	Lord Howe Rise	26° 06.70′ S	161° 13.60′ E	1533
DSDP590A	Lord Howe Rise	31° 10.02′ S	163° 21.51′ E	1299
DSDP591	Lord Howe Rise	31° 35.06′ S	164° 26.92′ E	2131
DSDP592	Lord Howe Rise	26° 28.40′ S	165° 26.53′ E	1088
DSDP593	Challenger Plateau	40° 30.47′ S	167° 40.47′ E	1068
DSDP284	Challenger Plateau	40° 30.48′ S	167° 40.81′ E	1066
DSDP594	Bounty Trough	45° 31.41′ S	174° 56.88′ E	1204
E13-3	Bellingshausen Basin	57° 00.00′ S	89° 29.00′ W	5090
E14-8	flank of Mid-Pacific Ridge	59° 40.00′ S	160° 17.00′ W	3875
INDIAN OCEAN				
V20-163	Mid-Indian Ridge	17° 12.00′ S	88° 41.00′ E	2706
V29-40	Mid-Indian Ridge	10° 29.00′ S	78° 03.00′ E	5325
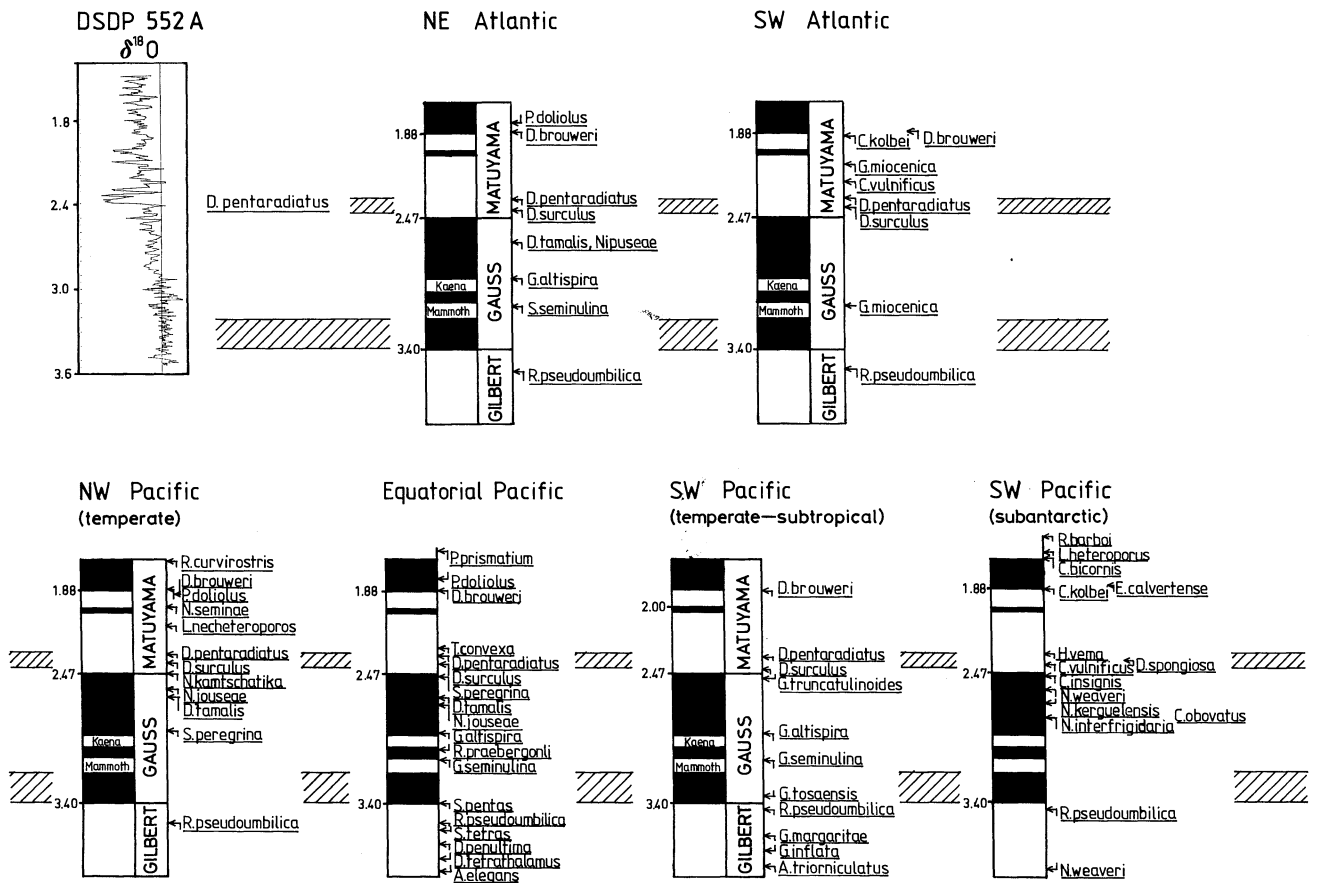
FIGURE 5. Standard stratigraphic sections showing the stratigraphic markers used in different parts of the ocean to define the two time intervals (hatched) described in this paper (table 2).

[83]

TABLE 2. SEDIMENT DATA FROM DSDP SITES AND PISTON CORES

site	average depth below sea floor (m) I	II	datums used for interval I	II	sedimentation rates (cm ka^{-1}) I	II	dry bulk density (g cm^{-3}) I	II	C_{org} (% by mass) I	II	C_{org} accum. rate (g cm^{-2} ka^{-1}) I	II	$CaCO_3$ (% by mass) I	II	$CaCO_3$ accum. (g cm^{-2} ka^{-1}) I	II	bulk accum. (g cm^{-2} ka^{-1}) I	II	PP_{new} (g cm^{-2} ka^{-1}) I	II
ATLANTIC																				
DSDP 552A	41.5	55.6	O-Rb	G/G-Mb	1.7 (1.6-1.8)	1.0 (1.0)	1.0	1.1	0.19	0.05	0.0033	0.0005	45.75	96.35	0.78	1.01	1.72	1.05	7.12	2.23
610A	123.5	165.8	Dp-Rb	G/G-Mb	5.3 (2.5-7.9)	2.9 (2.1-3.7)	—	—	0.18	0.08	0.0107	0.0025	72.00	88.18	4.27	2.73	5.93	3.10	14.68	6.29
611D	103.3	178.8	M/G-Rb	G/G-Mb	⟨5.9 (8.6-9.3)⟩	10.1 (9.4-10.7)	—	—	0.42	0.15	0.0317	0.0125	12.27	71.67	2.92	5.97	7.54	8.33	29.52	23.56
609B	165.2	241.8	Dp-Rb	G/G-Mb	10.2 (7.7-12.7)	5.0 (4.4-5.7)	—	—	0.24	0.06	0.0238	0.0033	58.70	90.01	5.81	4.91	9.91	5.46	35.05	9.43
548	130.7	178.7	Dp-Rb	—	5.7 (5.4-6.0)	—	1.3	—	0.36	—	0.0274	—	31.70	—	2.42	—	7.62	—	17.10	—
400A	123.1	161.0	Dp-Ob	G/G-Mb	3.8 (3.4-4.2)	3.2 (1.8-4.5)	1.3	—	0.49	0.20	0.0239	0.0067	30.20	55.50	1.48	1.87	4.89	3.37	42.21	21.58
608	80.9	108.5	Dp-Ob	G/G-Mb	3.1 (1.8-4.3)	0.9 (0.4-1.4)	—	—	0.03	0.03	0.0011	0.0003	95.00	97.31	3.36	0.99	3.54	1.02	4.69	2.16
607	105.6	141.8	Dp-Ob	G/G-Mb	5.2 (4.2-6.2)	3.0 (2.3-3.7)	—	—	0.04	0.04	0.0023	0.0014	88.00	94.18	5.04	3.39	5.73	3.60	7.45	5.48
606	76.3	113.8	O-Dp	G/G-Mb	8.5 (7.6-9.4)	7.3 (6.6-7.9)	—	—	0.11	0.04	0.0103	0.0035	94.55	97.52	8.89	8.56	9.41	8.78	17.76	8.51
397	179.5	272.2	O-Dp	G/G-Mb	9.2 (8.9-9.5)	4.9 (0.0-9.8)	—	—	0.94	0.44	0.0917	0.0315	44.75	65.00	4.37	4.66	9.76	7.17	70.92	34.96
141	22.6	41.2	O-Dp	G/G-O	4.1 (2.6-5.6)	⟨2.0 (1.9-2.1)⟩	1.0	1.1	0.05	0.08	0.0020	0.0018	79.90	82.62	3.18	1.83	3.97	2.22	8.20	7.67
541	106.3	138.0	Dp-Dp	G/G-Mb	2.5 (2.4-2.5)	0.9 (0.9)	—	—	0.13	0.14	0.0038	0.0015	43.00	45.00	1.27	0.48	2.95	1.08	14.23	6.00
366A	33.5	48.2	O-Dp	Rp-O	6.2 (6.0-6.3)	⟨2.3 (1.9-2.6)⟩	—	—	0.10	0.10	0.0022	0.0007	69.80	92.50	1.53	0.68	2.19	0.74	11.30	6.31
521	20.6	33.7	Dp-Ob	G/G-Mb	1.3 (1.1-1.5)	1.5 (1.5-1.6)	1.1	1.1	0.05	0.06	0.0007	0.0010	84.00	93.70	1.19	1.51	1.41	1.61	4.27	5.26
522	14.7	22.93	Dp-Ob	G/G-Mb	0.5 (0.1-0.9)	1.5 (1.3-1.8)	1.1	1.1	0.05	0.04	0.0003	0.0007	70.00	93.03	0.39	1.51	0.56	1.62	2.54	4.54
519	50.0	70.9	Dp-Ob	G/G-Mb	1.0 (0.7-1.2)	2.2 (1.7-2.6)	1.0	1.1	0.03	0.03	0.0003	0.0007	92.00	96.40	0.90	2.28	0.97	2.37	2.27	3.91
515A	50.2	—	M/G-Ob	—	⟨1.6 (1.6-1.7)⟩	—	—	—	0.33	—	0.0052	—	0.00	—	0.00	—	1.57	—	15.77	—
523	10.9	23.0	O-Dp	unclear	0.2 (0.1-0.3)	—	—	—	0.10	0.09	0.0002	—	90.00	—	0.16	—	0.18	—	2.31	—
518	21.6	33.6	Dp-Ob	G/G?-O	0.7 (0.7-0.8)	0.8 (0.7-0.9)	1.1	—	0.04	0.09	0.0003	0.0006	83.92	81.55	0.66	0.58	0.79	0.71	2.49	4.22
516A	10.4	17.7	—	G/G-Mb	—	0.8 (0.7-0.8)	—	1.1	0.12	0.08	—	—	—	94.42	—	—	—	—	—	1.58
517	30.5	42.0	—	G/G-Mb	—	1.9 (1.9-2.0)	—	—	0.12	0.12	—	—	82.50	83.80	—	—	—	—	—	6.01
514	41.4	—	M/G-Ob	unclear	⟨4.0 (4.0)⟩	—	—	—	0.30	—	0.0064	—	0.70	—	0.02	—	2.13	—	19.25	—
CARIBBEAN																				
502C	57.0	84.2	M21-Dp	G/G-Mb	9.4 (8.4-10.5)	2.8 (2.5-3.1)	0.8	1.0	0.31	0.29	0.0218	0.0082	49.00	48.80	3.81	1.39	7.78	2.84	31.98	16.23
PACIFIC OCEAN																				
V21-173	—	—	M/G-Ob	—	⟨4.4 (4.4)⟩	—	—	—	—	—	—	—	—	—	—	—	—	—	—	—
RC12-413	—	—	—	G/G-Mb	—	3.6 (3.6)	—	—	—	—	—	—	—	—	—	—	—	—	—	—
V21-148	—	—	M/G-Ob	G/G-Mb	⟨1.5 (1.5)⟩	5.2 (5.2)	—	—	—	—	—	—	—	—	—	—	—	—	—	—
RC10-203	—	—	M/G-Ob	—	⟨0.7 (0.7)⟩	—	—	—	—	—	—	—	—	—	—	—	—	—	—	—
DSDP580	—	—	M/G-Ob	—	⟨5.5 (5.5-5.4)⟩	—	—	—	—	—	—	—	—	—	—	—	—	—	—	—
RC12-415	—	—	M/G-Ob	G/G-Mb	⟨0.05 (0.05)⟩	—	—	—	—	—	—	—	—	—	—	—	—	—	—	—
V20-88	—	—	M/G-Ob	—	⟨0.2 (0.15)⟩	0.2 (0.2)	—	—	1.00	—	0.1200	—	0.00	—	—	—	12.20	—	114.36	—
DSDP440B	388.6	—	Dp-Db	unclear	9.9 (15.3-4.4)	unclear	—	—	—	—	—	—	—	—	—	—	—	—	—	—
DSDP579A	—	—	M/G-Ob	G/G-Mb	⟨3.8 (3.8-3.7)⟩	3.2 (3.9-2.6)	—	—	—	—	—	—	—	—	—	—	—	—	—	—
V20-89	—	—	M/G-Ob	G/G-Mb	⟨0.3 (0.25)⟩	0.1 (0.14)	—	—	—	—	—	—	—	—	—	—	—	—	—	—

Site			datum 1	datum 2	range 1	range 2														
DSDP310	29.8	46.6	O-Db	O-Gm	1.0 (1.2–0.9)	⟨2.1 (2.3–1.8)⟩	—	0.9	0.10	0.10	0.0009	0.0019	60.75	77.70	0.56	1.51	0.90	1.94	4.30	7.24
V32-127	—	—	Dp-Ob	—	0.3 (0.3–0.3)	—	—	—	—	—	—	—	—	—	—	—	—	—	—	—
DSDP578	—	39.2	M/G-Rb	G/C-Mb	⟨2.4 (2.35–2.4)⟩	1.1 (1.0–1.3)	—	—	—	—	—	—	—	—	—	—	—	—	—	—
DSDP577A	26.9	—	Dp-Ob	G/C-Mb	1.0 (0.8–1.2)	1.5 (1.4–1.6)	—	—	0.11	0.07	0.0010	0.0010	86.00	91.00	0.80	1.34	0.93	1.47	3.84	3.84
DSDP576	—	—	M/C-Ob	G/C-Mb	⟨0.4 (0.4–0.4)⟩	0.3 (0.3–0.35)	—	—	—	—	—	—	—	0.40	—	0.00	0.17	0.14	—	—
RC12-63	5.2	7.5	M/C-Ob	G/C-Mb	⟨0.2 (0.2)⟩	0.4 (0.4)	0.5	0.4	0.15	0.13	0.0010	0.0001	58.80	37.20	0.05	0.02	0.09	0.06	1.81	1.49
DSDP575	—	—	M/G-Ob	G/C-Mb	⟨0.2 (0.2–0.2)⟩	0.2 (0.1–0.2?)	0.5	0.4	0.21	0.16	0.0010	0.0001	30.20	46.80	0.08	0.13	0.28	0.28	4.31	3.90
V28-179	11.3	17.7	O-Ob	G/C-Mb	0.5 (0.5–0.5)	0.7 (0.7)	0.4	0.4	0.60	0.32	0.0006	0.0004	67.80	—	0.13	0.36	0.95	0.81	3.97	2.41
DSDP574	47.8	70.0	M/C-Ob	G/C-Mb	⟨0.5 (0.4–0.5)⟩	0.7 (0.6–0.8)	—	—	—	—	0.0006	0.0004	30.20	46.80	—	—	—	—	—	—
DSDP503B	—	M21-Ob	M21-Op	M21-Op	2.7 (2.6–2.9)	2.3 (1.9–2.6)	—	—	—	—	0.0057	0.0026	13.60	44.10	—	—	—	—	—	—
V24-62	—	—	G/C-Mb	0.5 (0.5)	0.3 (0.3)	—	—	—	—	—	—	—	—	—	—	—	—	—	—	—
V24-60	—	—	M/C-Ob	—	0.4 (0.4)	—	—	—	—	—	—	—	—	—	—	—	—	—	—	—
RC12-66	—	—	M21-Ob	M21-Ob	0.4 (0.4–0.4)	0.2 (0.2)	—	—	—	—	—	—	40.00	44.00	—	—	—	—	—	—
V24-59	—	—	M21-Ob	M21-Ob	0.3 (0.3–0.3)	0.2 (0.2)	—	—	—	—	—	—	—	—	—	—	—	—	—	—
KH68-4-18	87.6	152.5	M/C-Ob	M/C-Ob	⟨0.4 (0.4)⟩	—	0.5	0.7	1.76	0.16	0.0047	—	33.70	66.30	0.09	—	0.27	—	14.73	8.43
DSDP504	34.6	46.9	O-Ob	G/C-O	0.6 (0.6–0.7)	imprecise	0.7	0.6	0.18	—	0.0018	—	66.60	71.50	0.66	0.61	0.99	0.85	—	—
DSDP573	56.4	74.9	M/C-Ob	G/C-Mb	⟨1.5 (1.4–1.6)⟩	1.3 (1.2–1.4)	—	—	0.24	—	0.0064	—	88.00	—	2.34	—	2.65	—	7.94	—
DSDP586B	129.3	211.0	Dp-Db	unclear	2.7 (2.4–3.0)	unclear	0.6	—	0.70	—	0.0844	—	54.95	—	6.63	—	12.06	—	44.16	—
DSDP157	—	—	O-Tc	unclear	20.2 (19.5–21.0)	unclear	0.6	—	—	—	—	—	—	—	—	—	—	—	—	—
M70-39	—	—	—	G/C-Mb	—	0.6 (0.6)	—	—	—	—	—	—	—	—	—	—	—	—	—	—
KH68-4-20	—	—	—	G/C-Mb	—	1.1 (1.1)	—	—	—	—	—	—	—	—	—	—	—	—	—	—
M70-16	—	—	M/C-Ob	G/C-Mb	⟨0.2 (0.5)⟩	0.5 (0.5)	—	—	—	—	—	—	97.00	93.00	0.42	2.01	0.44	2.16	1.01	2.21
DSDP587	28.8	44.5	Dp-Db	G/C-Gs	0.4 (0.1–0.8)	⟨1.9 (1.5–2.3)⟩	—	—	—	—	—	—	96.60	94.80	0.53	1.78	0.58	1.88	4.14	6.59
DP588	46.1	75.4	Dp-Rb	G/C-Mb	0.5 (0.1–0.8)	1.6 (1.2–2.1)	—	—	0.05	0.05	0.0003	0.0009	91.00	92.60	2.28	5.78	2.50	6.24	7.41	11.30
DSDP590A	64.2	95.8	O-Ob	G/C-Mb	2.1 (1.9–2.3)	5.1 (4.8–5.3)	1.1	—	0.13	0.11	0.0033	0.0069	85.80	93.50	2.55	5.91	2.97	6.32	2.10	—
DSDP591	—	—	Dp-Ob	G/C-Mb	2.8 (2.4–3.2)	6.0 (5.8–6.2)	1.1	1.1	0.13	0.12	0.0039	0.0076	—	—	—	—	—	—	—	2.04
DSDP592	44.3	—	Dp-Ob	G/C-Gs	0.6 (0.4–0.8)	0.9 (0.0–1.8)	—	—	—	—	—	—	91.00	—	2.05	—	2.26	—	2.64	—
DSDP593	—	—	Dp-Ob	unclear	2.0 (1.8–2.2)	unclear	—	—	0.06	—	0.0014	—	87.00	90.00	—	—	—	—	—	—
DSDP284	50.0	78.0	Dp-Db	O-Rp	1.6 (1.4–1.8)	⟨1.0 (0.0–2.0)⟩	—	—	0.10	0.10	—	—	—	—	—	—	—	—	—	—
DSDP594	—	—	unclear	G/C-Mb	—	3.2 (3.1–3.3)	—	—	—	—	—	—	—	—	—	—	—	—	—	—
E13-3	—	—	Hv-Ob	G/C-Mb	⟨0.4 (0.4)⟩	0.4 (0.4)	—	—	—	—	—	—	—	—	—	—	—	—	—	—
E14-8	—	—	Hv-Ob	G/C-Mb	⟨0.4 (0.4)⟩	0.3 (0.3)	—	—	—	—	—	—	—	—	—	—	—	—	—	—
Indian Ocean																				
V20-163	—	—	—	G/C-Mb	—	3.9 (3.9)	—	—	—	—	—	—	—	—	—	—	—	—	—	—
V29-40	—	—	—	G/C-Mb	—	9.4 (8.9–10.00)	—	—	—	—	—	—	—	—	—	—	—	—	—	—

Abbreviations used for datums: Db, *D. brouweri*; Dp, *D. pentaradiatus*; G/G, Gauss–Gilbert; Gm, *G. margaritae*; Gs, *G. seminulina*; Hv, *H. vema*; M/G, Matuyama–Gauss; Mb, Mammoth base; O, oxygen isotope shifts at *ca.* 2.4 and 3.15 Ma BP; Ob, Olduvai base; Rb, Reunion base; Rp, *R. pseudoumbilicata*; Tc, *T. convexa*.

2.43–2.33 Ma BP, which represent two climatic extremes separated by an average $\delta^{18}O$ rise of 1.0–1.4 ‰ over approximately 0.75 Ma. We expect the preliminary distribution patterns of shifting accumulation rates to indicate the history of CO_2 chemistry during this important phase of climatic deterioration.

DATABASE AND DEFINITIONS

Figure 4 and table 1 *a* show the location of 66 drill holes, in which we were able to define our two time intervals: time interval II from 3.4 to 3.18 Ma BP and time interval I from 2.43 to 2.33 Ma BP. Time interval (slice) II averages the time range from the $\delta^{18}O$ minimum (i.e. the warm phase) immediately after the Gauss–Gilbert magnetic reversal until the top of the $\delta^{18}O$ minimum near the Mammoth magnetic event. Time interval (slice) I starts at the base of the first extreme cold stage near the last occurrence of *Discoaster surculus* and reaches to the top of this stage, ending just after the last occurrence of *D. pentaradiatus*. In addition to oxygen-isotope curves and well-calibrated microfossil datums, detailed $CaCO_3^-$ content curves were studied to determine the position of time intervals I and II in the cores (figure 5). Those cores for which palaeomagnetic and micropalaeontological datums suggest a hiatus for time slices I and II were not included in this study (figures 6*b*–9*b*). Bulk sedimentation rates for the two time slices were determined from those first-order age datums lying closest to the respective intervals (table 2).

From both time intervals, a total of about 500 samples from 31 selected core profiles in the Atlantic and Pacific Ocean were investigated for dry bulk density (DBD), calcium carbonate content, and organic carbon (% C) content, by means of standard laboratory techniques (Coulomat 702, Leco CS 244). By incorporating the respective bulk sedimentation rates (S_b), for the two time slices, we calculated the mass accumulation rates of the bulk sediment, carbonate sediment, and organic carbon. Figures 6–10 present average values for each time interval.

Furthermore, the new palaeoproductivity (P_{new}) (or 'export' productivity, from the surface ocean to the deep sea) of the ocean was calculated, based on the following assumptions.

(i) $P_{new} = P^2/400$, where P = primary production. Because this is a saturation function, $P_{new} = \frac{1}{2}P$ at more than $P = 200$ g m^{-2} a^{-1} (Eppley & Peterson 1979).

(ii) The accumulation rates of organic carbon (C_A) are considered as a function of P_{new}, the water depth (z) (Suess 1980) and the 'sealing effect', S_{b-c}). The latter is included in the calculation by using the (organic) carbon-free bulk sedimentation rate (Mueller & Suess 1979). According to Sarnthein *et al.* (1987*a*, *b*) we use the following equation for P_{new} (where D is the DBD):

$$P_{new} = 0.24\, C^{0.64} S_b^{0.86} D^{0.54}\, z^{0.83} S_{b-c}^{-0.24}\ (\text{g cm}^{-2}\ \text{a}^{-3}) \tag{1}$$

CHANGES IN THE SEDIMENT BUDGETS

From time interval II to time interval I the bulk sedimentation rates (figure 6*a*, *b*) and bulk accumulation rates (figure 7*a*, *b*) increased over large parts of the ocean. For example, in the north and equatorial Atlantic they increased by a factor of 1–3.5, in the equatorial eastern Pacific by a factor of 1–2, offshore from Japan by a factor of 1.2–2.5, and in the southern Pacific, south of 40° S, by a factor of 1–1.5. The rates generally decreased in the western
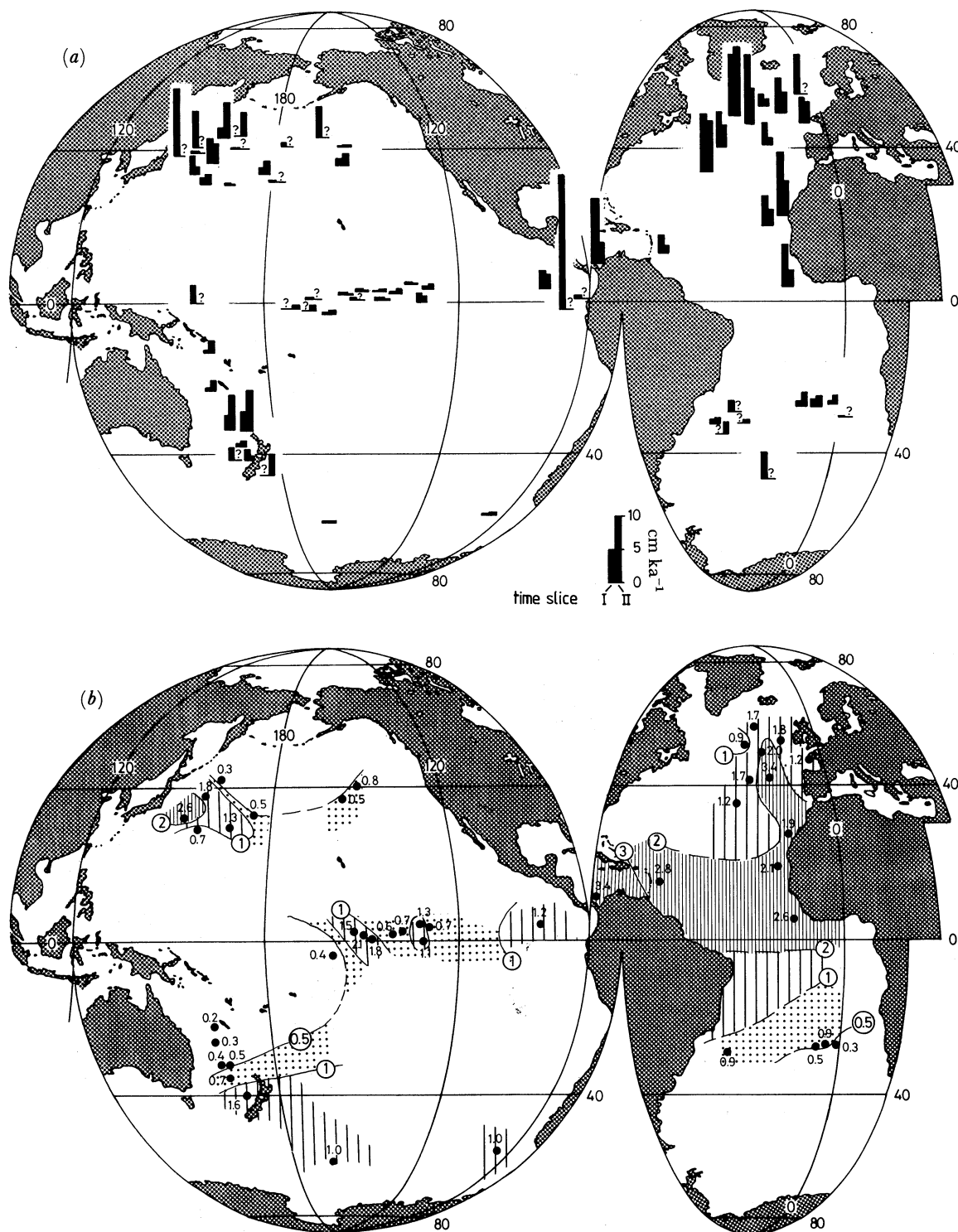
FIGURE 6. (a) Bulk sedimentation rates during time intervals I and II. ?, Hiatus and/or imprecise chronostratigraphy. (b) Change of bulk sedimentation rates from time interval II to time interval I (by factor x; > 1.0 = increase; < 1.0 = decrease).
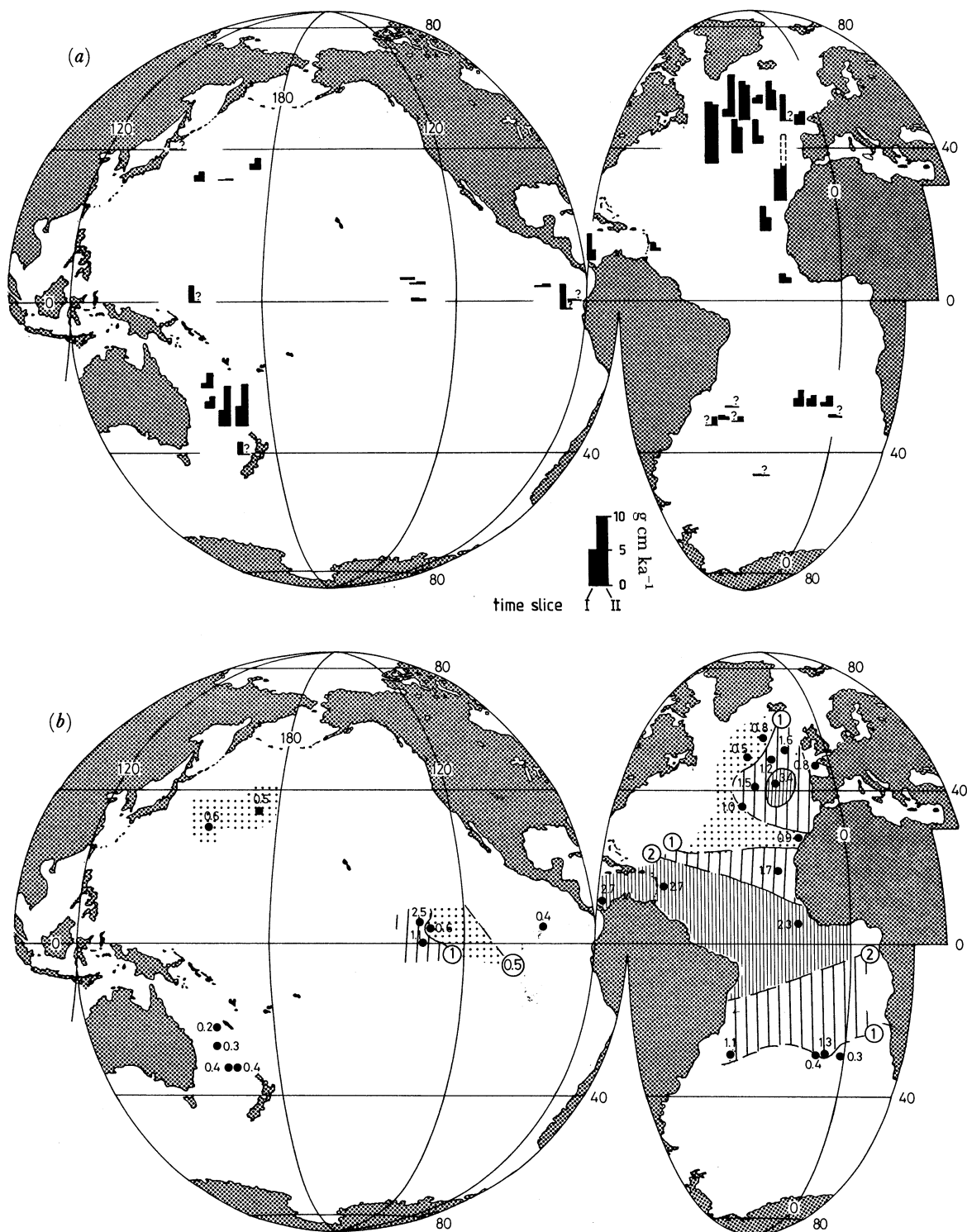
498 M. SARNTHEIN AND J. FENNER

FIGURE 7. (a) Bulk accumulation rates during time intervals I and II. ?, Hiatus and/or unprecise chronostratigraphy. (b) Change of bulk accumulation rates from time interval II to time interval I (by factor x).

FIGURE 8. (a) CaCO$_3$ accumulation rates during time intervals I and II. ?, Hiatus and/or imprecise chronostratigraphy. (b) Change of CaCO$_3$ accumulation rates from time interval II to time interval I (by factor x).

500   M. SARNTHEIN AND J. FENNER

equatorial and southwestern Pacific north of 40° S, in the central north Pacific, and in most of our south Atlantic sections (by a factor of 0.3–0.9).

This pattern is much better understood in combination with the distribution pattern of $CaCO_3$ accumulation rates (figure 8a, b). From time interval II to I, they decrease in most parts of the Pacific (factor 0.2–0.6) and in large parts of the Atlantic (factor 0.2–0.9). Increases in the $CaCO_3$ accumulation rate are confined to the equatorial Atlantic, parts of the equatorial Pacific, and the Caribbean (factor 1.1–3.3), and to the North Atlantic off west Europe (factor 1.0–3.4), possibly also to the Vema Gap.

Accordingly, the increase of bulk accumulation and sedimentation rates found in the easternmost equatorial and in the northwest Pacific, in the eastern subtropical and northern Atlantic, and probably also that in the south Pacific, must be the result of a strongly enhanced terrigenous (siliciclastic) sediment discharge, which also enhances the bulk sediment-accumulation rates in the equatorial Atlantic beyond the increase observed for the $CaCO_3$ accumulation. Biogenic opal, a third variable, is not quantitively crucial where measured in these areas.

These findings are in accord with the late Pliocene increase in Saharan dust output and aridity as reported by Stein (1984, 1985) from sites 141 and 397. Similarly, they match an enhanced inner Asian dust discharge found by Leinen & Heath (1981) and Rea & Janecek (1982) in North Pacific sediments. Furthermore, they agree with the increased deposition rate of ice-rafted debris reported from site 552 (Zimmerman et al. 1985), a depositional process probably also contributing to the slight increase of sedimentation rates in the South Pacific.

The late Pliocene increase of $CaCO_3$ deposition near the equator may largely reflect enhanced local $CaCO_3$ production (see below). This can be concluded from the fact that the average $CaCO_3$ accumulation rates strongly decreased in most non-equatorial parts of the Atlantic and Pacific oceans (figure 8) (see also recent results from ODP leg 108 in Ruddiman et al. (1987)). Accordingly, they indicated that the deep ocean water in general became more corrosive to $CaCO_3$ during that time and that any local lowering of the carbonate compensation depth (CCD) was due to locally enhanced $CaCO_3$ fluxes. Possible explanations for this will be discussed below.

A fairly simple pattern emerges from the late Pliocene shift of accumulation rates of organic carbon (C_A) (figure 9). They decrease over almost all the Pacific and South Atlantic ocean, and in the Caribbean Sea (factor 0.3–0.7; with the exceptions of the region east off Japan and the equatorial Pacific). Simultaneously, the rates increase all over the North Atlantic, being especially strong near the equator and in the West European basin (factor 2.5–6.0). This general pattern may be meaningful, in spite of the still very thin data coverage available, because the various core locations were selected to represent the most characteristic high and low ocean productivity zones in middle and low latitudes.

Accordingly, we observe a global shift in the deposition of organic carbon, away from the low-productive subtropical gyres in the Pacific and South Atlantic towards the equatorial high-productivity belt and in particular, towards the North Atlantic. Besides changes in surface ocean productivity (figure 10), this increase in C_A may be due to the increased sedimentation rates (figure 6), especially in the North Atlantic, which have led to an enhanced 'sealing effect' for the carbon flux arriving on the sea floor. On the other hand, reduced ventilation of the deep
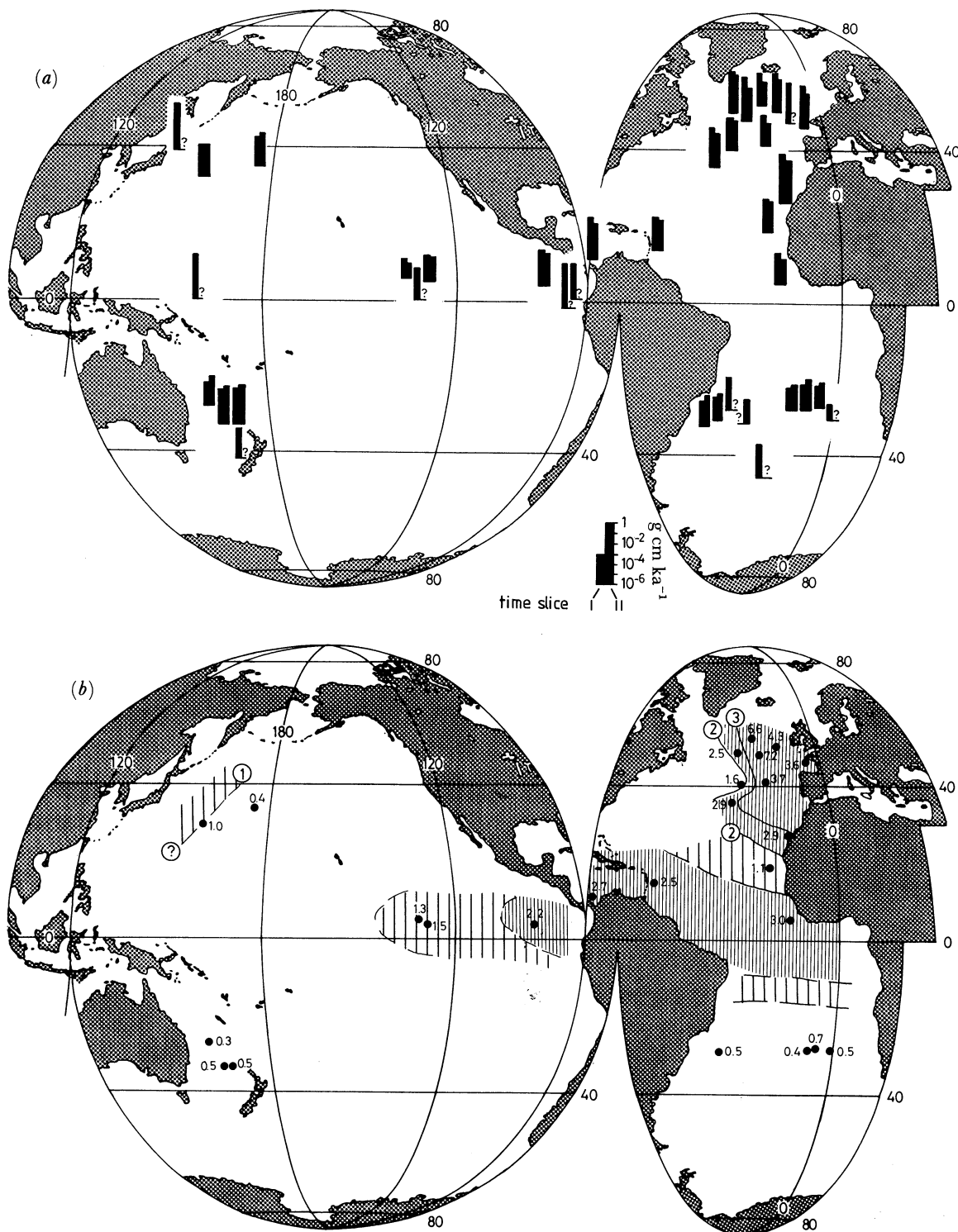
[90]

FIGURE 9. (a). Accumulation rates of organic carbon during time intervals I and II. ?, Hiatus and/or imprecise chronostratigraphy. (b) Change of C_{org} accumulation rates from time interval II to time interval I (by factor x).
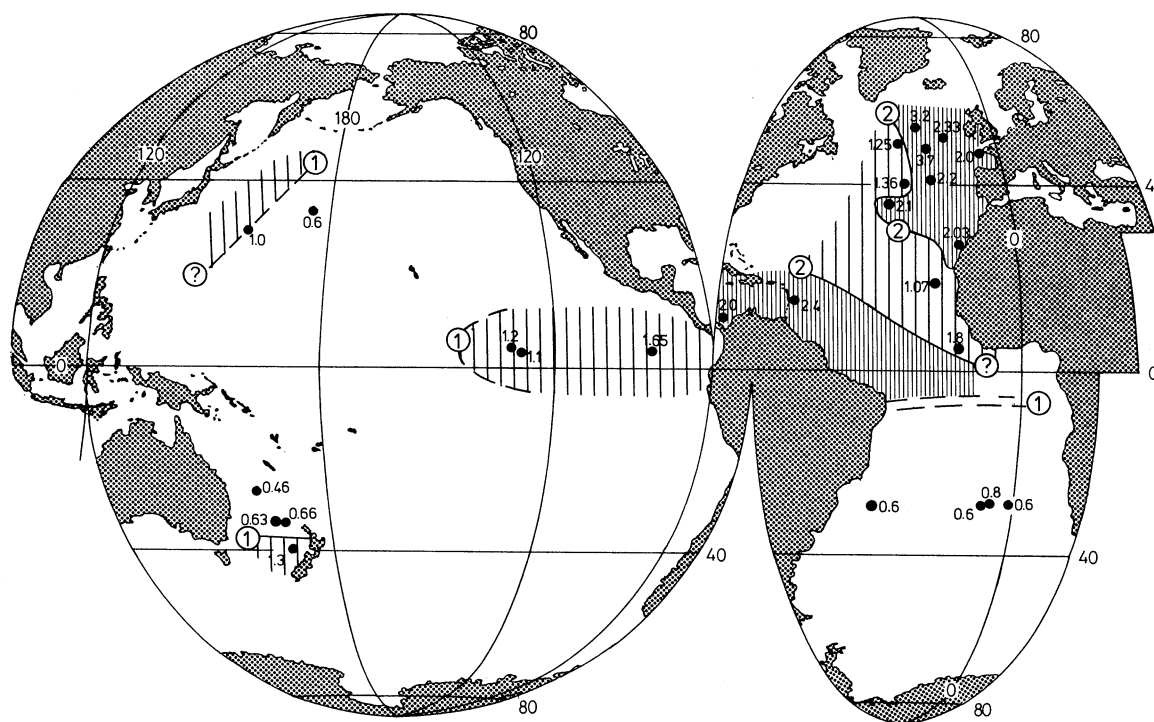
[91]

FIGURE 10. Increase in new palaeoproductivity from time interval II to time interval I (by factor x).

sea can be hardly considered as a possible cause, because Suess (1980) and Sarnthein et al. (1987) have shown that the oxygen concentration in the bottom water does not control C_A as long as it exceeds ca. 50–100 μmol kg^{-1}.

CHANGES IN OCEAN PRODUCTIVITY

In absolute terms, the new productivity at 3.4–3.18 Ma BP lies within a range of 1.5–71.0 g cm^{-2} ka^{-1} and thus appears markedly lower than that of today (as recalculated after Eppley & Peterson (1979), from Koblentz-Mishke et al. (1970), and Romankevitch, (1984)), by a factor of up to more than 10. The values from time interval I, 2.43–2.33 Ma BP, lie somewhat closer to the present ones. However, this direct comparison of numbers from the present and the past is probably deceptive, because our data were not subjected to any correction for the long-term diagenetic loss of carbon from deep-sea sediments (compare Mueller et al. (1983)).

Nevertheless, the palaeoproductivity shift from time interval II to I (figure 10) will be essentially independent of this diagenetic imprint because only minor differences in sediment thickness are involved. As a result, we observe a productivity increase covering the southwesternmost and northwesternmost Pacific and the upwelling belt of the eastern equatorial Pacific (factor of 1.0–1.65). Ocean productivity has increased much more (by a factor of 1.1–3.7) in the equatorial Atlantic, the Caribbean Sea, the west-European–Iberian Sea, and the coastal upwelling region off northwest Africa. The latter can be taken as a representative example for the four great, trade-wind driven near-shore upwelling belts along the eastern continental margins of the Atlantic and Pacific in the subtropics. On the other

hand, regions with decreasing palaeoproductivity occur in the midlatitudinal south Atlantic, northern and southwestern Pacific (factor of 0.6–0.8). In summary this means that the low productivity of 'blue' ocean regions in the subtropical gyres further decreased and simultaneously, the high productivity in the 'green' ocean regions further increased, i.e. the whole productivity pattern was more polarized 3.2–2.4 Ma BP.

DISCUSSION

From the distribution and pattern of palaeoproductivity increases, we may infer that the upwelling in the eastern equatorial Pacific and along the eastern margins of the Pacific and Atlantic Oceans was markedly intensified during the late Pliocene phase of global climatic deterioration. Based on the evidence from increasing grain sizes of the aeolian dust discharge in the low-latitudinal east Atlantic (Stein 1985) (figure 2), this intensification of upwelling was probably controlled by strongly enhanced meridional trade-wind speeds (by a factor of about 3), i.e. a wind régime already coming close to that of the Last Glacial Maximum. The wind-induced, intensified upwelling, in turn, led to reduced sea-surface temperatures in low latitudes, and hence to reduced evaporation. Accordingly, enhanced oceanic upwelling was probably crucial for the large-scale aridification of the Saharan belt, observed during that time (Sarnthein et al. 1982; Stein 1985) (figure 2).

The most important implication of the increased ocean productivity is to be expected in the field of ocean and atmospheric chemistry. We may conclude that the enhanced new production led to a globally increased rate of carbon extraction from the surface ocean (and hence the atmosphere) to the deep ocean on the order of magnitude of that observed about 20 ka ago, during the Last Glacial Maximum (Sarnthein et al. 1988). This late Quaternary shift resulted in a decrease of the atmospheric p_{CO_2} from an interglacial level of about 300 p.p.m (by volume) down to about 200 p.p.m. (by volume) (Delmas et al. 1980). A similar somewhat more modest shift may be now conceivable for the late Pliocene phase of climatic deterioration, implying a feedback loop of further climate cooling. This assumption is in accord with the independent evidence obtained from benthic $\delta^{13}C$ values, showing a lowering of about 0.25 ‰ and thus an increased storage of CO_2 in North Atlantic Deep Water during that time, as outlined in the Introduction (figure 3). Furthermore, this enhanced storage of CO_2 in the deep ocean is in general agreement with the record of stronger $CaCO_3$ dissolution in large parts of the ocean and also with the locally enhanced rates of $CaCO_3$ accumulation found immediately below the equatorial high productivity zones (figure 7). They indicate a local increase of $CaCO_3$ fluxes paralleled by a generally enhanced carbonate aggressivity of the bottom water.

REFERENCES

Delmas, R. J., Ascensio, J.-M. & Legrand, M. 1980 Polar ice evidence that atmospheric CO_2 20,000 yr BP was 50% of present. *Nature, Lond.* **284**, 155–157.
Duplessy, J. C. 1982 North Atlantic deep-water circulation during the last climatic cycle. *Bull. Inst. Geol. Bassin d'Aquitaine, Bordeaux* **31**, 379–391.

Eppley, R. & Peterson, B. J. 1979 Particulate organic matter flux and planktonic new production in the deep ocean. *Nature Lond* **282**, 677–680.

Koblentz-Mishke, O. J., Volkowinsky, V. V. & Kabanova, J. G. 1970 Plankton primary production of the World Ocean. In *Scientific exploration of the South Pacific* (ed. W. S. Wooster), pp. 183–193.

Leinen, M. & Heath, G. R. 1981 Sedimentary indicators of atmospheric activity in the northern hemisphere during the Cenozoic. *Palaeogeogr. Palaeoclim. Palaeoecol.* **36**, 1–21.

Mueller, P., Erlenkeuser, H. & Grafenstein, R. V. 1983 Glacial–Interglacial cycles in oceanic productivity inferred from organic carbon contents in eastern North Atlantic sediment cores. In *Coastal upwelling: its sediment record* (ed. J. Thiede & E. Suess), part B, pp. 365–398.

Mueller, P. & Suess, E. 1979 Productivity, sedimentation rate, and sedimentary organic matter in the oceans. I. Organic carbon preservation. *Deep Sea Res.* A**26**, 1347–1362.

Rea, D. K. & Janecek, T. R. 1982 Mass-accumulation rates of the non-authigenic inorganic crystalline (eolian) component of deep-sea sediments from the western Mid-Pacific Mountains, Deep Sea Drilling Project Site 463. *Init. Rep. DSDP*, vol. 62 (ed. J. Thiede, T. L. Vallier *et al.*), pp. 653–659. Washington, D.C.: U.S. Government Printing Office.

Romankevich, E. A. 1984 *Geochemistry of organic matter in the ocean.* Heidelberg: Springer-Verlag. (334 pages.)

Ruddiman, W., Sarnthein, M., Baldauf, J. *et al.* (eds.) 1987 *Init. Rep. DSDP*, vol. 108, part A. Washington D.C.: U.S. Government Printing Office.

Sarnthein, M., Thiede, J., Pflaumann, U., Erlenkeuser, H., Fuetterer, D., Koopmann, B., Lange, H. & Seibold, E. 1982 Atmospheric and oceanic circulation patterns off NW-Africa during the past 25 million years. In *Geology of the Northwest African Continental Margin* (ed. U. v. Rad, K. Hinz, M. Sarnthein & E. Seibold), pp. 545–604. Berlin: Springer-Verlag.

Sarnthein, M., Winn, K., Duplessy, J.-C. & Fontugne, M. R. 1988 Global variations of surface ocean productivity in low and mid latitudes: influence on CO_2 reservoirs of the deep ocean and the atmosphere during the last 21,000 years. *Palaeoceanography.* (Submitted.)

Sarnthein, M., Winn, K. & Zahn, R. 1987 Paleoproductivity of oceanic upwelling and the effect on atmospheric CO_2 and climatic change during glaciation times. In *Abrupt climatic change* (ed. W. H. Berger & L. D. Labeyrie), pp. 311–337. Dordrecht: D. Reidel Co.

Shackleton, N. J. & Hall, M. A. 1985 Oxygen and carbon isotope stratigraphy of Deep Sea Drilling Project Hole 552 A: Plio-pleistocene glacial history. *Init. Rep. DSDP*, vol. 81 (ed. D. G. Roberts, D. Schnitker *et al.*), pp. 599–610. Washington D.C.: U.S. Government Printing Office.

Shackleton, N. J. & Cita, M. B. 1979 Oxygen and carbon isotope stratigraphy of benthic foraminifers at site 397: detailed history of climatic change during the late Neogene. *Init. Rep. DSDP*, vol. 47, pp. 433–445. Washington, D.C.: U.S. Government Printing Office.

Stein, R. 1984 Zur neogenen Klimaentwicklung in Nordwest-Afrika und Palaeo–Ozeanographie im Nordost-Atlantik: Ergebnisse von DSDP Sites 141, 366, 397 und 544 B. *Berichte-Reports, geol. palaeont. Inst. Univ. Kiel*, vol. 4 (210 pages.)

Stein, R. 1985 Late Neogene changes of paleoclimate and paleoproductivity off Northwest Africa (DSDP Site 397). *Palaeogeogr. Palaeoclim. Palaeoecol.* **49**, 47–59.

Suess, E. 1980 Particulate organic carbon flux in the oceans surface productivity and oxygen utilization. *Nature, Lond.* **288**, 260–263.

Zahn, R., Winn, K. & Sarnthein, M. 1986 Benthic foraminiferal $\delta^{13}C$ and accumulation rates of organic carbon: *Uvigerina peregrina* group and *Cibicidoides wuellerstorfi. Paleoceanography* **1**(1), 27–42.

Zimmerman, H. B., Shackleton, N. J., Backman, J., Kent, D. V., Baldauf, J. G., Kaltenback, A. J. & Morton, A. C. 1985 History of Plio-Pleistocene climate in the northeastern Atlantic, Deep Sea Drilling Project Hole 552 A. *Init. Rep. DSDP*, vol. 81 (ed. G. D. Roberts, D. Schnitker *et al.*), pp. 861–876. Washington, D.C.: U.S. Government Printing Office.